Multiphoton time-domain fluorescence lifetime imaging microscopy: practical application to protein–protein interactions using global analysis

P. R. Barber[1,*,†], S. M. Ameer-Beg[1,2], J. Gilbey[1], L. M. Carlin[2],
M. Keppler[2], T. C. Ng[2] and B. Vojnovic[1,†]

[1]*University of Oxford Gray Cancer Institute, Mount Vernon Hospital,
Middlesex HA6 2JR, UK*
[2]*King's College London, Randall Centre, New Hunt's House, Guy's Medical School Campus,
London SE1 1UL, UK*

Förster resonance energy transfer (FRET) detected via fluorescence lifetime imaging microscopy (FLIM) and global analysis provide a way in which protein–protein interactions may be spatially localized and quantified within biological cells. The FRET efficiency and proportion of interacting molecules have been determined using bi-exponential fitting to time-domain FLIM data from a multiphoton time-correlated single-photon counting microscope system. The analysis has been made more robust to noise and significantly faster using global fitting, allowing higher spatial resolutions and/or lower acquisition times. Data have been simulated, as well as acquired from cell experiments, and the accuracy of a modified Levenberg–Marquardt fitting technique has been explored. Multi-image global analysis has been used to follow the epidermal growth factor-induced activation of Cdc42 in a short-image-interval time-lapse FLIM/FRET experiment. Our implementation offers practical analysis and time-resolved-image manipulation, which have been targeted towards providing fast execution, robustness to low photon counts, quantitative results and amenability to automation and batch processing.

**Keywords: fluorescence lifetime; time-correlated single-photon counting;
time-domain fluorescence lifetime imaging microscopy; Förster resonance energy transfer;
global fitting**

1. INTRODUCTION

Identifying specific cellular protein–protein interactions in space and time, and elucidating their function, are now of great importance in the post-genomic era. Such interactions occur over a spatial distance of a few nanometres, placing heavy demands on any experimental technique that may be capable of resolving them. The detection of Förster (or fluorescence) resonance energy transfer (FRET) is one such technique, which is sensitive at these small distance scales (Voss *et al.* 2005; Wallrabe & Periasamy 2005). FRET can be detected optically and used to monitor protein interactions if the proteins are conjugated with suitable donor and acceptor fluorophores, such that the fluorescence emission spectrum of the donor overlaps the absorption spectrum of the acceptor and their dipoles align. The interaction, detected optically via FRET, can be localized with a spatial accuracy of a few hundred nanometres.

FRET depletes the excited state population of the donor reducing the intensity and the lifetime of the donor fluorescence. It is well known that the efficiency of energy transfer between these fluorophores varies as the inverse sixth power of the distance between acceptor and donor (Lakowicz 1999). The advantages of using donor fluorescence lifetime to detect FRET via fluorescence lifetime imaging microscopy (FLIM) as opposed to intensity based methods (Jares-Erijman & Jovin 2006) are the independence of the measurement to fluorophore concentration and light path as well as removing the need to make numerous normalizing measurements to obtain a quantitative result (Jares-Erijman & Jovin 2006). It is therefore well suited to studies in intact cells (Ng *et al.* 1999; Wouters *et al.* 2001).

*Author for correspondence (paul.barber@rob.ox.ac.uk).
[†]Present address: Gray Institute of Radiation Oncology and Biology, University of Oxford, Churchill Hospital, Oxford OX3 7DQ, UK

FLIM may be achieved by several methods that include: time-correlated single-photon counting (TCSPC) in the time domain (Tadrous 2000; Ameer-Beg *et al.* 2002; Chen & Periasamy 2004; Becker *et al.* 2006) and the frequency-domain method (Gadella *et al.* 1993; Bastiaens & Squire 1999; Lakowicz 1999). When TCSPC is used, the sample is excited repeatedly with delta-like pulses of light, and the time delays between these pulses and fluorescence photons emitted by the sample are measured, thus building a record of the transient fluorescence response of the sample. The exciting light is focused to record the response at a single point, which is then scanned over the sample to record an image. The frequency domain method often involves illuminating the sample with sinusoidally modulated light and recording the fluorescence signal emitted. Measurement of the phase shift and demodulation of the signal owing to the sample enables its lifetime to be determined. When several modulation frequencies are employed more than one lifetime may be determined. We choose to use TCSPC owing to its increased sensitivity over frequency-domain techniques, allowing modest illumination powers to be used (Gratton *et al.* 2003). Time-domain FLIM has been frequently used in the context of biological microscopy and there are many examples in the literature (Peter & Ameer-Beg 2004; Voss *et al.* 2005; Festy *et al.* 2007; Hille *et al.* 2008; Liu *et al.* 2008). Although, frequency-domain FLIM allows for simpler experimental set-ups, it has a more limited temporal dynamic range, unless multiple modulation frequencies are used. However, the accuracy of the results is ultimately determined by the linearity of the demodulation process (Mizeret *et al.* 1999). Moreover, frequency-domain techniques generally require high signal intensities and are less appropriate for operation in a photon counting mode. Conversely, TCSPC methods are generally limited in their maximal counting rates and are thus more appropriate when signal intensities are low. The efficiency of photon usage is best described using the 'figure of merit' (F; Gerritsen *et al.* 2002; Philip & Carlsson 2003); for TCSPC, this is near to unity while it is typically poorer for frequency domain methods.

Quantifying the interacting sub-population of donor-labelled proteins is an important aim of an inter-molecular FRET experiment. The reduction in lifetime due to FRET is dependant on the FRET efficiency and therefore, on the separation of the donor and acceptor fluorophores (Lakowicz 1999). Since there will be a distribution of separations for the ensemble of donor molecules, it would be most appropriate to consider the fitting of a complex distributed lifetime model to the transient fluorescence signal and recover the distance distribution of fluorophores (Rolinski *et al.* 2000). However, given the complexity of this approach, the need for extremely high photon counts to achieve statistically relevant results and the almost on/off nature of the sixth power dependence on distance, it is reasonable to assume that only two populations of donor molecules are present, i.e. interacting and non-interacting. This is particularly, relevant in experiments that involve fluorophores that exhibit

mono-exponential decays as it allows the use of a bi-exponential model to analyse these two populations. The experiments in this paper use green fluorescent protein (GFP) as the FRET donor that does exhibit a mono-exponential decay under our preparation protocols in live cells (see the electronic supplementary material and Ameer-Beg *et al.* (2003) and Parsons *et al.* (2005)), despite some reports to the contrary when measured in solution. Many studies can be performed while meeting this requirement for a mono-exponential donor. Newer fluorescent proteins (Shaner *et al.* 2005) may not exhibit mono-exponential decay kinetics and would require more complex fitting models that are also implemented using our global methods. Similar complex models may be required in cases where significant autofluorescence is present. In our experience with live and fixed cell work this has not been required. Since short acquisition times are desirable in most biological applications, a good photon economy is required. In practice, the most widely used time-resolved detectors are photomultiplier tubes (Becker 2005) and their quantum efficiency peaks in the green part of the spectrum, and are therefore well matched to GFP.

Previously, the analysis of FLIM/FRET data at low photon counts has been often hampered by the use of mono-exponential lifetime decay models that cannot distinguish the interacting fraction of donor–acceptor pairs from the FRET efficiency. In a mixed population, where there is a distribution of molecular separations or unbound donor fluorophores, multiple exponential decay kinetics are most likely observed. A high FRET efficiency arising from a low concentration of interacting molecules may lead to the incorrect assumption that there is little or no interaction. The FRET efficiency and interacting fraction can be resolved with the use of a bi-exponential model. Extracting additional parameters with statistical significance places greater demands on the accuracy of the data, and appropriate signal-to-noise levels must be maintained. One must be especially careful where a technique such as TCSPC is used. This is often count-rate-limited and the major noise contribution thus has a Poisson statistical nature. In general, a total photon count of 1000 would provide a good mono-exponential fit whereas nearer 10 000 counts are required to fit a bi-exponential model (Kollner & Wolfrum 1992). The latter may increase substantially under practical conditions where background counts are above zero or where the difference in component lifetimes is small.

This work describes and explores fitting mono- and bi-exponential models to real and simulated transient data. We use a *global* fitting algorithm that can be used to relax the signal-to-noise requirements at individual image points, and combine the data from the whole image or multiple images, retaining the spatial and temporal resolution, under the assumption that the donor lifetimes of the interacting and non-interacting populations are constant. It has previously been demonstrated that the meaning of global from 'all pixels in one image' can be expanded to 'all pixels in an experiment' (Clayton *et al.* 2004). In this paper,

we demonstrate the practical use of the modified Levenberg–Marquardt (MLM) algorithm as part of a practical and 'biologist friendly' software tool, in fixed and live-cell examples, extending it to multi-image global analysis and building upon a preliminary publication that was based on simulated data (Barber *et al.* 2005) and several detailing practical application (Ameer-Beg *et al.* 2002, 2003, 2005; Parsons *et al.* 2005; McConnell *et al.* 2007; Prag *et al.* 2007; Levitt *et al.* 2008).

There have been reports of the application of global analysis to time-domain data (e.g. Beechem & Haas 1989), but applications to time-domain FLIM have been limited. One such application relied on the combination of data from segmented image regions to obtain good initial estimates and speed up the iterative fitting procedure (Pelet *et al.* 2004). Although, in some cases, that approach has merit, the work described here uses significant optimizations for fitting exponential decay functions, such that model convergence occurs quickly (in several seconds for a typical image) without region-based assumptions, by using the rapid lifetime determination (RLD; Sharman *et al.* 1999) method to achieve good initial lifetime estimates. Others have shown an increased performance with low-photon-count data through the use of maximum-likelihood techniques (Bajzer *et al.* 1991).

Global analysis has previously been used to extract bi-exponential information from frequency-domain techniques (Verveer & Bastiaens 2003) in which single, or limited, frequency data can be used to extract FRET efficiency and population information if similar assumptions about constant lifetimes across the sample are made. Other authors have explored the benefits of graphical methods (Clayton *et al.* 2004) and techniques based on lifetime moments (Esposito *et al.* 2005). One technique that has been proposed to deal with complex multi-exponential decays, without the need for fitting, is the phasor plot (Digman *et al.* 2008), which can be applied to both time and frequency-domain data. This technique, although a powerful visual tool (Wouters & Esposito 2008), and useful at low photon counts, requires further processing if quantitative or automated results are required. This may involve fitting a non-linear distribution function to the two-dimensional data clouds. Under typical experimental conditions, one is usually faced with images of low signal-to-noise ratio (i.e. due to low fluorophore concentrations and the requirement for low pixel dwell times when imaging live cells) that makes these techniques, including those using other transforms (e.g. Laplace, Fourier or Laguerre) somewhat unsuitable to our problem (Pelet *et al.* 2004). Although, the benefits of global techniques can also be harnessed with such transforms (Jo *et al.* 2005).

The techniques presented in this paper are complementary to those works but are applied to the analysis of time-domain data. Similar numerical techniques (e.g. Marquardt minimization) and assumptions (e.g. constant image lifetimes) are often used in both domains. All techniques, including the work presented here, require that there is sufficient variation in populations across the sample (a low interacting

fraction, less than 0.2, can be tolerated as long as areas of higher fraction, more than 0.5, are also present) and that there is sufficient difference in component lifetimes. It is these aspects that are explored in this text. However, a most important aspect of FLIM is that a single image consists of several hundred thousand decay curves that must be analysed and therefore speed and amenability to automation are key to the practical application of the fitting algorithm and the software application that embeds it. We have concentrated on an algorithm that is fast, provides quantitative results, is readily used in automated systems or batch processing and robustly handles time-resolved images with low-photon counts.

2. MATERIAL AND METHODS

2.1. *Time-domain multiphoton FLIM*

Time-domain FLIM was performed with two multi-photon microscopy systems. System 1 (Ameer-Beg *et al.* 2002), was based on a modified MRC 1024MP workstation (Bio-Rad, Hemel Hempstead, UK), Millenia X and Tsunami 3941S femtosecond self-mode-locked Ti:Sapphire laser (Spectra Physics Lasers, Inc., Mountain View, CA, USA), TE300 microscope body (Nikon Instruments Europe B.V., The Netherlands) and SPC730 TCSPC electronics (Becker & Hickl, Berlin, Germany). System 2, was based on a Mira Ti:Sapphire laser (Coherent, Santa Clara, CA, USA), a TE2000 microscope body (Nikon), an in-house developed scan head, SPC830 single-photon counting electronics (Becker & Hickl) and a temperature controlled enclosure. Non-descanned detection was afforded in both systems by the use of fast single-photon response, photomultiplier tubes (7400 series, Hamamatsu Ltd., Japan) situated in the re-projected pupil plane of the objective. The instrument responses were measured from the hyper-Rayleigh scattering of highly attenuated excitation in a suspension of 20 nm colloidal gold (G-1652, Sigma-Aldrich Company Ltd, Dorset, UK; Habenicht *et al.* 2002) and found to be approximately 170 ps full width at half maximum and these measured responses were used in the fitting of data. Photons were collected at 500 nm (filter 35-5040, Coherent). The laser power was adjusted to give average photon counting rates of the order 10^4–10^5 photons s^{-1} and with peak rates approaching 10^6 photons s^{-1}, below the maximum counting rate afforded by the TCSPC electronics to avoid pulse pile-up (Becker 2005). The photon arrival times, with respect to the approximately 80 MHz repetitive laser pulses, were binned into 64 or 256 time windows over a total measurement period of 10 ns. Images were captured with a 40× objective lens (Plan Fluor 40×/1.3 oil, Nikon) at either 128×128 or 256×256 pixels, with imaged areas of 67×67 or 157×157 μm, respectively.

2.2. *Analysis of FLIM data*

The following bi-exponential fluorescence decay model was fitted to the data by iterative reconvolution

(Grinvald & Steinberg 1974; Periasamy 1988)

$$I_c(t) = Z + I_0 \int_{-\infty}^{\infty} I_{instr}(t - t') \cdot (\alpha_1 \exp(-t/\tau_1)$$
$$+ \alpha_2 \exp(-t/\tau_2)) dt', \qquad (2.1)$$

where
$$\alpha_1 + \alpha_2 = 1, \qquad (2.2)$$

and $I_{instr}(t)$ is the instrumental response; I_0 is the peak intensity; α_1 and α_2 are the fractional proportions of the lifetimes, τ_1 and τ_2, respectively. The same equation with $\alpha_2 = 0$ was used for the mono-exponential model. The reduced goodness-of-fit parameter, χ_r^2, was used as defined by

$$\chi_r^2 = \frac{\sum_{k=1}^{n} \frac{[I(t_k) - I_c(t_k)]^2}{I_c(t_k)}}{n - p}, \qquad (2.3)$$

where $I(t_k)$ is the data and $I_c(t_k)$ the fit value at the kth time point, t_k; n is the number of time points; and p the number of variable fit parameters. Normalizing by the value of the fit ($I_c(t_k)$), rather than the data ($I(t_k)$) in equation (2.3) leads to less-biased estimates, especially when photon counts are low (Sharman *et al.* 1999). χ_r^2 was minimized using a modified MLM algorithm (Levenberg 1944).

Assuming the second exponential component relates to the interacting population, we use the following definition of FRET efficiency:

$$\eta_{FRET} = 1 - \frac{\tau_2}{\tau_1}. \qquad (2.4)$$

The interacting fraction is simply given by α_2. This differs from the usual definition of fractional contribution for populations of mixed species, which equates the *area* under the transient ($\alpha_i \tau_i$) to the number of molecules. This is not generally appropriate for the detection of energy transfer as the two populations will have different quantum yields but the fact that they have the same *radiative* lifetime allows the comparison of signal amplitudes (Lakowicz 1999).

The MLM algorithm is sensitive, in both the result and the speed of convergence, to the prior estimated parameters that are used to initiate it, as others have found (e.g. Pelet *et al.* 2004). Key to our algorithm is the use of the RLD method (Woods *et al.* 1984; Sharman *et al.* 1999) to estimate these initial parameters. The RLD method is based on the fact that a good estimate of the lifetime of a single exponential decay can be obtained by performing three integrals over the decay curve. The result is somewhat sensitive to the time intervals that define these integrals and our algorithm optimizes these by iteratively decreasing the intervals from 1/3 of the total recorded time, to 1/4, 1/5, 1/6, 1/8, 1/10, etc., while the χ_r^2 continues to fall (always using the first three neighbouring time intervals nearest the start of the transient). If the decay is complex and not mono-exponential in form, then an 'average' lifetime results from RLD. In our implementation of MLM, this average lifetime is used to derive the initial guesses for each of lifetimes required by the current fitting model (i.e. based on the RLD result τ_{RLD}, $\tau_1 = \tau_{RLD}$, $\tau_2 = 2 \times \tau_{RLD}/3$, $\tau_3 = \tau_{RLD}/3$, where τ_i is the lifetime of the ith exponential component in a multi-exponential decay).

From the initial guesses the algorithm iterates, using the Levenberg–Marquardt method, to reduce χ_r^2. Iteration continues until $\chi_r^2 < 1.5$ or 10 consecutive iterations do not reduce the χ_r^2 (i.e. a change less than 10^{-7} as single-precision floating point numbers are used). An estimate of the error in the fitted parameters is calculated based on the shape of the χ_r^2 landscape, but the accuracy of this error varies depending upon the number of iterations used to reach an acceptable χ_r^2 minimum. More of the χ_r^2 landscape or 'support plane' can be calculated if required but we have found that more reliable estimates of practical errors are obtained from Monte Carlo type experiments with simulated data as presented in this paper.

Our MLM algorithm is embedded in the software application named time-resolved imaging, which is at its second major release (TRI2). This implements a user interface and code framework that enables the use of mono-, bi-, tri- and stretched-exponential models that allow for experiments using fluorophores with complex decays or where there may be interfering autofluorescence (Benny Lee *et al.* 2001). The application is based around a flexible image viewing and manipulation framework that includes pre-processing (e.g. pixel binning), batch processing, χ_r^2 support plane analysis, macro abilities and image processing functions for three-dimensional time-resolved data (figure 1). A copy of the executable program is available on request from the authors. Details of image storage, processing and presentation can be found in the electronic supplementary material.

2.3. Global analysis

The above analysis may be performed on each pixel of the image in turn (pixel-by-pixel analysis where we make no spatial or temporal restraints on the fitting parameters), but in addition it may be extended to analyse all pixels globally under the assumption that the lifetimes of interacting and non-interacting species, and therefore the FRET efficiency, are constant across all pixels (global analysis; Verveer *et al.* 2000). The signal-to-noise ratio of the data is critical in determining parameter accuracy (Eaton 1990; Istratov & Vyvenko 1999; Lakowicz 1999; Gratton *et al.* 2003); global analysis exploits the Poissonian nature of TCSPC data to obtain robust lifetime estimates but also allows fractions (α_1 and α_2) to vary on a pixel-by-pixel basis. The entire dataset is considered simultaneously to minimize a global χ^2 value.

Both the individual pixel and global fitting algorithms use the nonlinear least-squares method, based on the χ^2 gradient. The constant lifetime assumption results in a significant speed-up in execution of the global algorithm. The modifications in this MLM algorithm are the pre-calculation of many differentials, as well as their convolutions with the instrument response reduce significantly the number of calculations that need to be performed for each pixel. The use of the RLD method for parameter estimation from three areas under the transient is used to provide initial parameter estimation, speeding up convergence. The memory requirements are surprisingly modest as the most
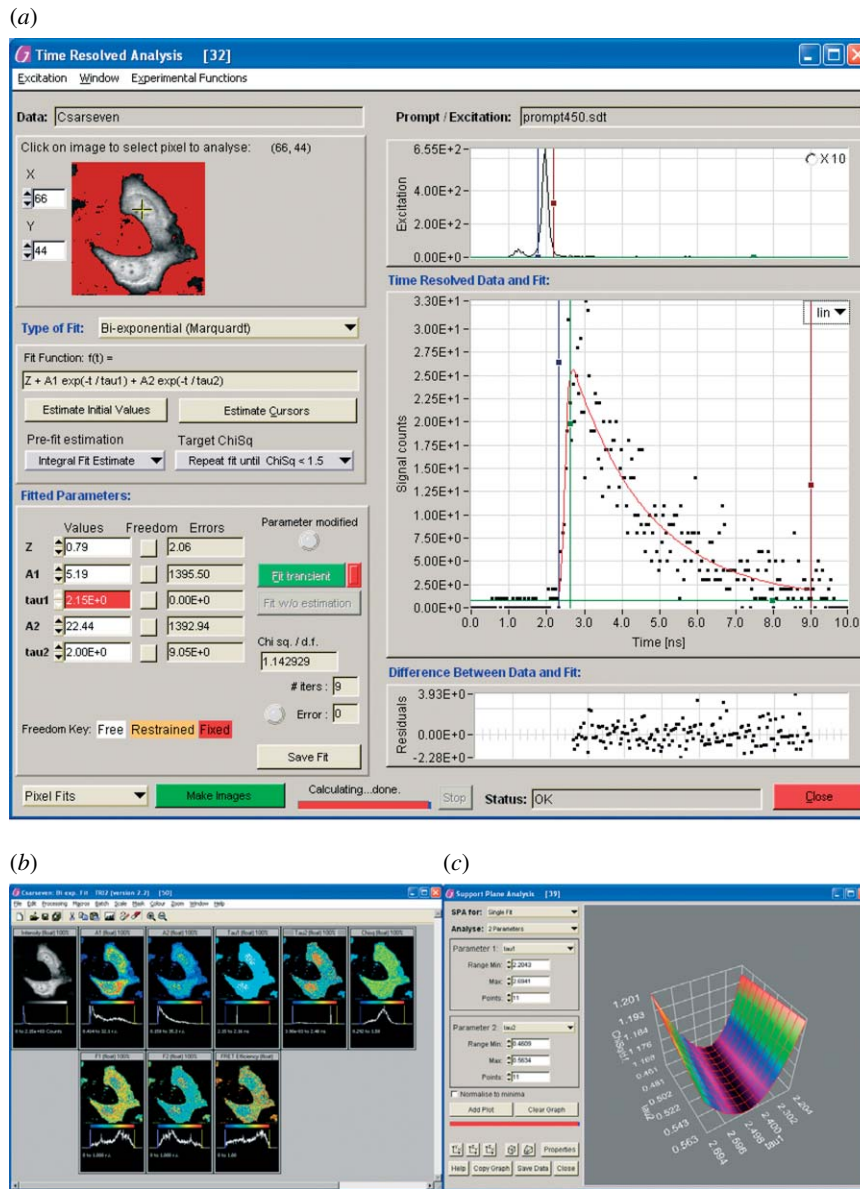
(*a*)

(*b*)   (*c*)

Figure 1. Screenshots from the time-resolved analysis program, TRI2. (*a*) The data from a point, selected from the image (top left), displayed on a graph together with a fit to the data (right-hand side). In the lower left of this panel the fitted parameters are shown. The parameter in red has been fixed by the user for this particular fit. (*b*) The framework image viewer and parametric images produced as a result of a bi-exponential fit to every pixel in an image. Macros have been implemented to calculate the interacting fractions (*F*) and the FRET efficiency based on the fit results. The 'support plane' functions for exploring the change in χ_r^2 as a function of fitted parameters is shown in (*c*).

memory hungry part of the algorithm, optimizing amplitude parameters for each individual pixel, is essentially linear owing to global lifetime values. On a 32-bit Windows computer, the 2 GB per process memory limit will allow the global analysis of approximately 120 images (256×256 pixels by 64 time points). These optimizations formed the basis for our implementation of the global least-squares approach and the mathematical detail on our implementation of this global analysis method can be found in a previous publication (Barber *et al.* 2005).

2.4. Simulated transient generation

The fitting algorithms were tested with simulated data of the expected signal from a model of the TCSPC system. Unlike other simulations, we included the fact

that the excitation laser operates at a pulse repetition rate of approximately 80 MHz, in the following simple manner. If the pulses are separated by *T* seconds, then (Barber *et al.* 2005)

$$ I(t) = Z + I_0 \sum_{i=1}^{m} R_i \alpha_i \exp(-t/\tau_i), \qquad (2.5) $$

where

$$ R_i = 1 + \frac{1}{\exp(T/\tau_i) - 1}. $$

This raw fluorescence signal was convolved with a Gaussian excitation pulse and simulated Poisson noise was added to simulate real photon counts. All simulated data included both a fixed background and the effect of repetitive excitation.

3. RESULTS

The performance of the MLM fitting algorithms for both pixel-by-pixel and global analysis has been explored with simulated data previously (Barber *et al.* 2005). With global analysis of a 32×32 pixel image, the error in extracted mono-exponential lifetime was lower than 0.4 per cent for signals with a peak of 500 photon counts or more, over the lifetime range 0.5–3.0 ns (640–3840 total counts per pixel). The fitting model and method could fit mono-exponential lifetimes up to 20 ns (with less than 5 per cent error in the recovered lifetime) by adequately estimating the fixed background from the post-pulse data. In this regime, the effects of a repetitive excitation do not preclude fitting of such long lifetimes and throughout our analysis the use of the time window prior to the pulse to estimate any fixed background was not used, nor should it be owing to the possible effect of repetitive excitation.

Bi-exponential decays were also modelled in order to simulate a FRET experiment with GFP as the donor ($\tau_1 = 2.15$ ns) and a peak photon count of 500. Provided the lifetime of GFP undergoing FRET was below ≈ 1 ns ($\eta_{\mathrm{FRET}} > 0.5$), an interacting population of 10 per cent could be accurately characterized. There was, however, increasing difficulty in determining the interacting fraction as this lifetime increased above ≈ 1.6 ns ($\eta_{\mathrm{FRET}} < 0.25$). Introducing the concept of an apparent FRET efficiency ($\eta_{\mathrm{AP}} = \eta_{\mathrm{FRET}} \times \alpha_2$), we can say that good results are obtained when $\eta_{\mathrm{AP}} > 0.2$, with this number of counts. This definition of η_{AP} is useful as it approximates the effective FRET efficiency measured when a mono-exponential fitting model is used (see below).

Additional simulated data and two experiments demonstrating the performance with fixed and live cell data now follow.

3.1. Comparison between pixel-by-pixel and global analysis: simulated data

Figure 2 offers a visual indication of the performance when fitting a bi-exponential for a particular FRET pair and expresses the results in terms of FRET efficiency and interacting fraction. A theoretical FRET pair with an unquenched donor lifetime of 2.1 ns and a quenched lifetime of 0.4 ns was chosen. We compare mono- and bi-exponential models, fitted by pixel-by-pixel and global algorithms. In the sample image, the bi-exponential amplitudes vary from 0 to 1000 counts independently and linearly from left to right for component 1 and top to bottom for component 2 giving rise to the intensity pattern of figure 2*a*.

The RLD method alone gives a fast result but one which is biased to lower apparent FRET efficiency. Mono-exponential pixel-by-pixel MLM fits are three times slower to calculate than RLD but offer a more robust result. Bi-exponential MLM fits reveal the interacting fraction as well as FRET efficiency; pixel-by-pixel fits taking five to seven times longer than RLD. A bi-exponential global MLM fit takes only 30 per cent longer than RLD and reveals the cleanest result. The exponential component amplitudes recovered

from the simulated data are given in figure 2*h*,*i* and these clearly show the variation in these parameters. With simulated data, it is possible to get good estimates of the error in the parameters determined through repeated experiments with independent noise. The lifetime values determined by global analysis, over eight experiments, were 2.100 ± 0.002 ns and 0.400 ± 0.001 ns (mean $\pm$ s.d.), and $\eta_{\mathrm{FRET}} = 0.809 \pm 0.002$.

If the FRET efficiency is known, or can be estimated, prior to analysis then an interacting fraction can be inferred from a mono-exponential model. In figure 3, we show this and compare it to bi-exponential fitting for a system similar to figure 2 ($\tau_1 = 2.1$ ns, $\tau_2 = 0.4$ ns). Mathematically, one can define two average lifetimes for bi-exponential data (Lakowicz 1999); both are weighted averages of the component lifetimes. The lifetime can be weighted by its fractional contribution:

$$\overline{\tau} = \frac{\sum \alpha_i \tau_i^2}{\sum \alpha_j \tau_j}, \tag{3.1}$$

or by its fractional amplitude

$$\langle \tau \rangle = \sum \alpha_i \tau_i, \tag{3.2}$$

where τ represents a lifetime and α the corresponding component proportions (see §2). In our experience, the measured lifetime from fitting a mono-exponential model to bi-exponential data using MLM and RLD is always between these two values, but usually closer to the average weighted by the fractional amplitude. The estimation of the FRET efficiency from this average lifetime is poor when the interacting fraction is low, being only correct when $\alpha_2 = 1.0$.

First, the theoretical FRET efficiency was calculated for both cases corresponding to equations (3.1) and (3.2), lifetime weighted by contribution or by amplitude. These are the solid and dotted lines in figure 3, respectively. The ideal result is a constant line at 0.81 ($= 1 - 0.4/2.1$). This effective FRET efficiency calculated using the amplitude weighted lifetime is equivalent to the apparent FRET efficiency, η_{AP}, defined above. Then mono-exponential model fits, using both RLD and MLM algorithms, were applied to simulated data. The results are overlaid on to figure 3 in green and red. It can be seen that the MLM determined values lie close to those derived from *amplitude-weighted* lifetimes. The RLD data lie on a number of lines due to the optimization algorithm attempting to find the best widths for the integration periods (lines correspond to integration bins that are 1/3 and 1/4 of the transient's duration). The results of fitting a bi-exponential model are also presented (yellow and black; the black is often obscured by the yellow in figure 3*b*). A global bi-exponential fit produces good and constant lifetimes and a line at a FRET efficiency of 0.81 (black).

Pixel-by-pixel bi-exponential fits (yellow) suffer when the interacting fraction is very small or very large (i.e. fits are good when $0.2 < \eta_{\mathrm{AP}} < 0.7$). This is due to the signal representing one lifetime, swamping the other and precluding its accurate determination. Global analysis obviously wins here as it has good
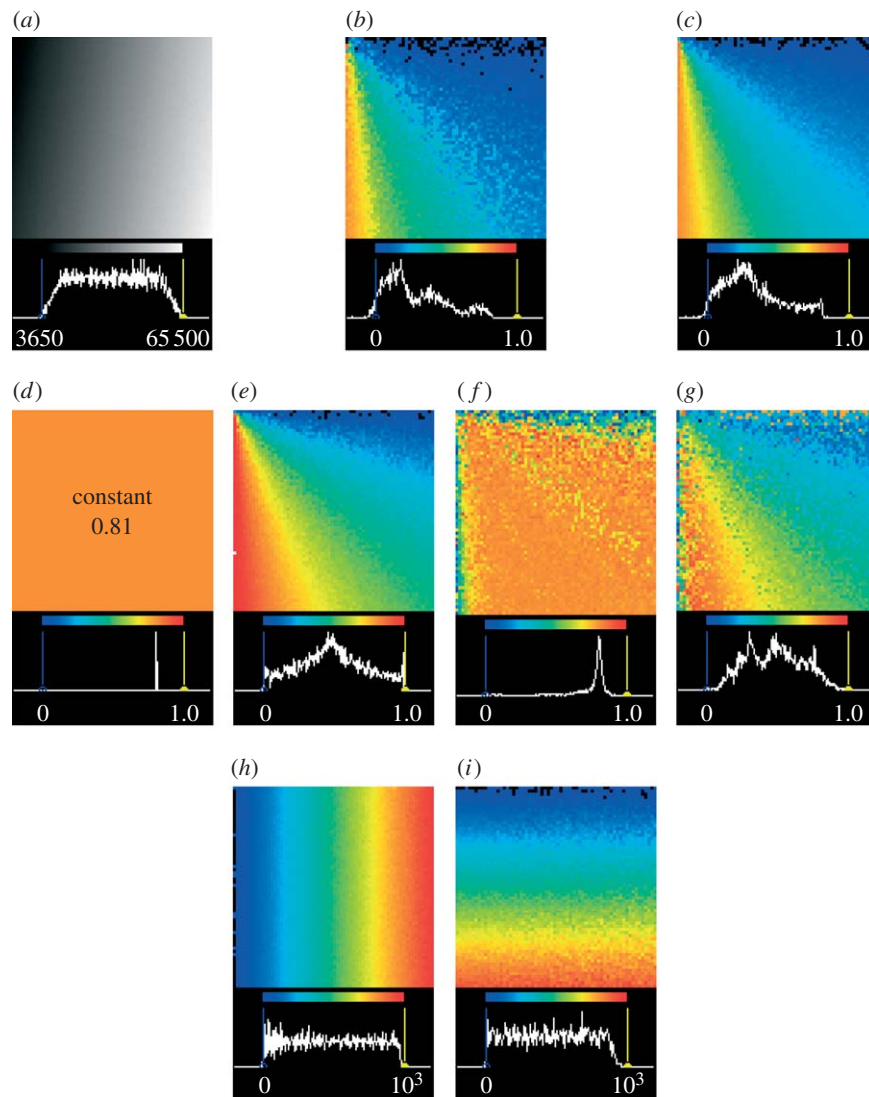
Figure 2. Comparing mono- and bi-exponential models fitted by pixel-by-pixel and global algorithms to simulated data. (*a*) Total intensity image. (*b,c*) FRET efficiency from RLD and mono-exponential global MLM fits. FRET efficiency and interacting fraction maps, respectively, from (*d,e*) bi-exp global and (*f,g*) bi-exp pixel fits. (*h,i*) The component amplitudes recovered using a global bi-exponential fit and the recovered lifetimes, 2.100 and 0.401 ns. The true lifetimes used to generate the data were 2.100 and 0.400 ns (FRET efficiency = 0.81). Below each image is its histogram over the pixel intensity range shown.

estimates of lifetimes, derived from the whole image at all values of η_{AP}. This analysis indicates that great care must be taken when applying bi-exponential fits on a pixel-by-pixel basis, owing to this failure at low and high interacting fractions. Indeed, mono-exponential fits provide a more robust analysis provided it shortcomings are understood (cf. figure 2*b,c,e,g*).

If the unquenched lifetime can be determined from areas of the image where its signal amplitude is good, then its value can be fixed, and pixel-by-pixel bi-exponential fits perform much better in the high-interacting-fraction regime; however, selecting portions of the image is hard to automate. Furthermore, if this unquenched lifetime can be determined from an independent sample, an attempt can also be made to determine FRET efficiency *and* interacting fraction from fitting a mono-exponential model by calculating FRET efficiency from the lowest observed average lifetime and then using equations (2.2) and (3.2) to calculate α_2 (figure 3*b*). This allows fast RLD type

techniques to be used that would be more robust than bi-exponential pixel fitting at the extremes of interacting fraction (e.g. $\eta_{AP} < 0.2$ or $\eta_{AP} > 0.7$ in this case).

3.2. Comparison between pixel-by-pixel and global analysis: cell data

As an example of the efficacy of global fitting, we have applied it to an experiment to image the interaction of a neural Wiskott–Aldrich syndrome protein (N-WASP) with protein Cdc42 (Parsons *et al.* 2005). Cells were microinjected with plasmids encoding GFP-N-WASP and HA-tagged WT or N17 inactive mutant Cdc42, fixed, and stained with a Cy3-conjugated anti-HA IgG Fab fragment. Multiphoton donor FLIM was undertaken on System 1 to determine the extent of FRET between GFP-N-WASP (donor) and anti-HA-Cy3 (acceptor). Acquired images consisted of 128×128 pixels and 256 time bins. Figure 4 shows a series of images that compare the results of pixel and global fits to mono- and bi-exponential models. Acceptor-absent
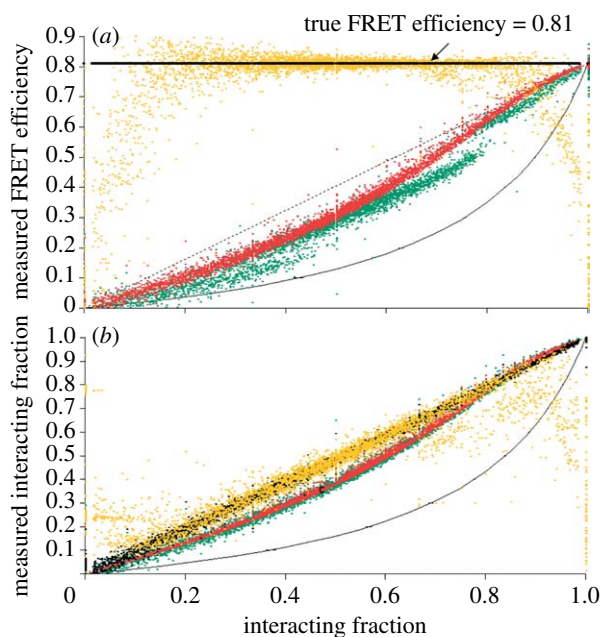
Figure 3. (*a,b*) Comparing the measured (dots) or calculated (lines) FRET efficiency and interacting fraction for RLD, mono- and bi-exponential MLM fits, using both pixel-by-pixel and global algorithms on the simulated data of figure 1. From the estimates of FRET efficiency measured by a mono-exponential MLM fit (*a*: red dots) one sees that the recovered lifetime resembles that of a theoretical average lifetime derived by weighting by the fractional amplitudes (*a*: dashed line). With this information, and assuming a FRET efficiency *a priori*, a good estimate of the interacting fraction can be made (*b*: red dots), which is often better than pixel-by-pixel bi-exponential fits (*b*: yellow dots), and RLD (*b*: green dots). However, bi-exponential fits (yellow dots) produce the correct result for FRET efficiency and interacting fraction over a limited range of true interacting fractions without assumptions about the FRET effciency. Only global analysis (black dots) gives the correct result over the whole range of interacting fractions. All data are simulated. See text for a detailed explanation. $\tau_1 = 2.1$ ns, $\tau_2 = 0.4$ ns in all cases; signal amplitudes range from 0 to 2000 counts. Green dots, RLD; red dots, mono-exp MLM; black dots, bi-exp global MLM; yellow dots, bi-exp MLM; solid line, contribution weighted calculated values; dashed line, amplitude weighted calculated values.

control cells were used to verify and measure the unquenched GFP lifetime. The mean lifetime from the control (2.18 ns) was fixed as a parameter in the bi-exponential fits.

Figure 4*b,c* shows that using mono-exponential analysis, FRET is detected, with an effective FRET efficiency of approximately 0.3. If we move to a bi-exponential model, we are able to calculate an interacting fraction, which, together with the calculated FRET efficiency, is shown in figure 4*f,g*, respectively. When using global fitting (figure 4*d,e*) constant lifetimes are assumed across the dataset and the calculated FRET efficiency is constant at a value of near 0.63. The main differences between the histograms produced by global and pixel fitting are explored in figure 4*j*. Pixel-by-pixel fitting results in a population of pixels showing an interacting fraction near 1.0 which are clearly artefactual (black area). These are

due to insufficient representation of the unquenched lifetime component, resulting in near mono-exponential data and ill-defined bi-exponential fits at these pixels. These rogue pixels contribute to the extremes of the FRET efficiency histogram (black area), the remaining pixels are clustered around the global analysis result of 0.63.

3.3. Comparison between pixel-by-pixel and multi-image global analysis: time-lapsed cell data

It is often beneficial in time-lapse experiments to acquire images with a short intervening time interval such that a higher temporal resolution can be maintained. This results in a limited period for photon accumulation and low-photon-count images. We performed the following experiment to demonstrate the robust estimation of lifetimes from such data while maintaining temporal and spatial resolution.

The Rho family of small GTPase proteins (Cdc42, Rac and Rho) integrate changes in the extra or intracellular environment and transduce them to downstream effectors (Ridley 2006). The Rho GTPase Cdc42 has been implicated in organization of the actin cytoskeleton (Hall 1998), especially the production of filopodia (Kozma *et al.* 1995). Here, the human epithelial carcinoma cell line A431 was stimulated with epidermal growth factor (EGF) and Cdc42 activity monitored using the FRET probe Raichu-Cdc42 (Nakagawa *et al.* 1998; Itoh *et al.* 2002), which was adapted to make it suitable for two-photon FLIM by forming a GFP-Raichu-mRFP1 probe (see the electronic supplementary material). Cells were imaged on System 2 at 1 frame (256×256 pixels by 64 time bins) approximately every 15 s for several frames and then recombinant human EGF-biotin (Invitrogen) was added to the medium to a final concentration of 10 ng ml^{-1}. Any changes in focal plane were then compensated for and the cell imaging continued (see the electronic supplementary material).

If the spatial distribution of the interaction is of no interest (or is assumed irresolvable for experimental reasons) then lifetime invariant fits (where all data in the image or series of images is summed and fitted for an average lifetime or lifetimes) is of use. Figure 5*a* shows the time course of average lifetime from mono-exponential invariance fits. A bi-exponential lifetime invariant fit of the whole dataset revealed an interacting lifetime of 1.36 ns, and similar analysis of control data revealed a non-interacting lifetime of 2.41 ns (see the supplementary data); this slightly increased GFP lifetime was found to be consistent across live cell experiments. These values can be used as fixed parameters for further image by image, bi-exponential, lifetime invariant fits. This analysis is presented in figure 5*b* and reveals the time course of interacting fraction. If the resolution of spatial information is desirable then binned pixel-by-pixel fitting can be performed, again by using the two lifetimes determined by invariant fits as fixed parameters; this is presented in figure 5*c*. Use of a multi-image global fit by-passes
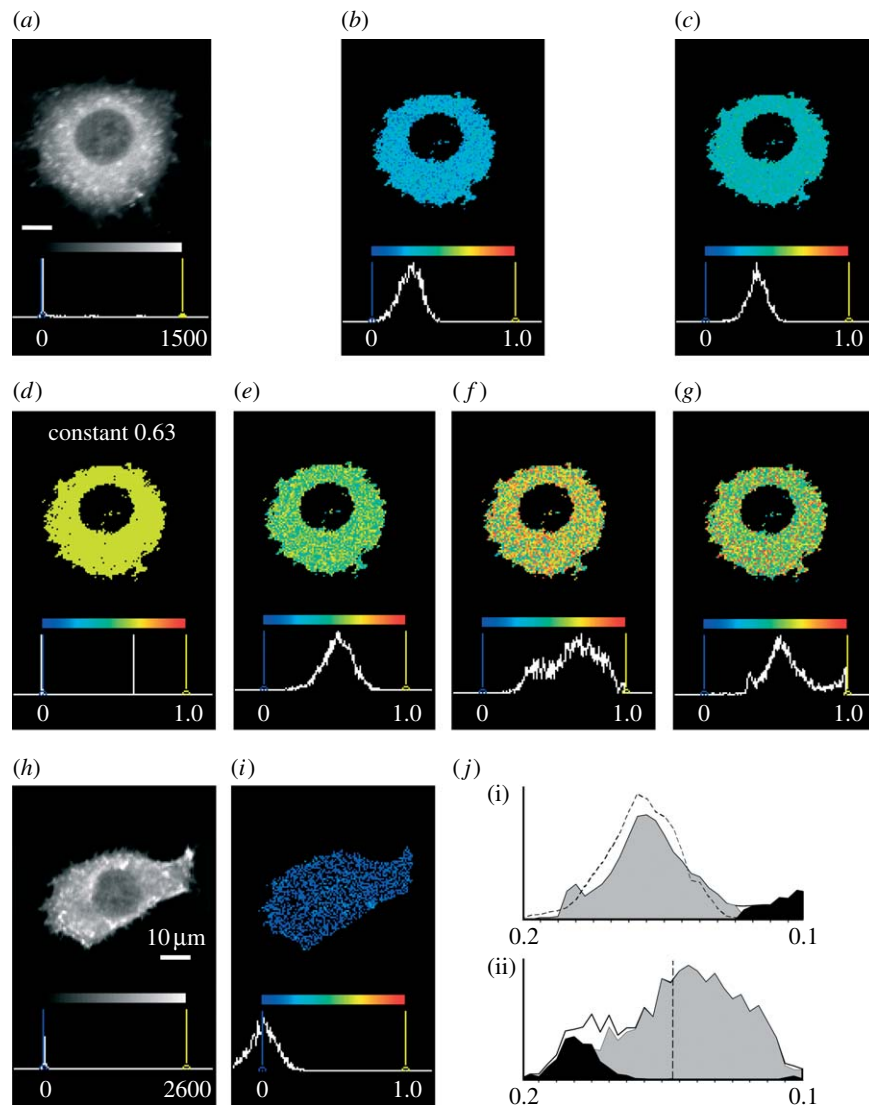
Figure 4. Comparing mono- and bi-exponential models fitted by pixel-by-pixel and global algorithms to cell data. (*a*) Total intensity image. (*b, c*) FRET efficiency from RLD and mono-exponential global MLM fits. FRET efficiency and interacting fraction maps, respectively, from (*d, e*) bi-exp global and (*f, g*) bi-exp pixel fits. (*h, i*) Control cell intensity and FRET efficiency. Below each image is its histogram. (*j*(i)) Interacting fraction and (ii) FRET efficiency histograms. Solid lines, pixel-by-pixel analysis; dotted lines, global analysis. Black area, poorly fitted pixels due to insufficient representation of the unquenched lifetime component, resulting in near mono-exponential data and artefacts due to ill-defined bi-exponential fits at these pixels. Grey area, pixels with a good bi-exponential fit.

many of these steps, reveals an interacting lifetime of 1.39 ns and the time course of interacting fraction, in agreement with other observations (Kurokawa *et al.* 2004), and in a approximately one-fifth of the calculation time (figure 5*d*).

4. DISCUSSION

In §3, the power and potential shortcomings of MLM fitting have been represented, and the additional benefits offered by global analysis have been demonstrated. Inferring the FRET efficiency from a fit to a mono-exponential model can be extremely misleading as only the average lifetime can be calculated, but such a fit may be of use if it is well understood.

The time required to process the data from an area of an image similar to a typical cell (4000 pixels, 0.5 μm

per pixel scale) on a pixel-by-pixel basis varied from approximately 2 s for RLD fits to 16 s for bi-exponential MLM fits, with global bi-exponential analysis taking 3 s. All measurements were taken on an Intel P4 2.4 GHz PC (see table 1 in the electronic supplementary material). This global fitting technique is fast to calculate owing to the optimizations that can be made when fitting exponential data (see §2). Further speed-up could be achieved through the use of multithreading as algorithms of this type can be made highly parallel.

Therefore, the method of choice for deriving the FRET efficiency and interacting fraction is global fitting of a bi-exponential model which provides both these quantities automatically, using only the data from the current image. The fact that robust estimates of FRET efficiency and interacting fraction can be
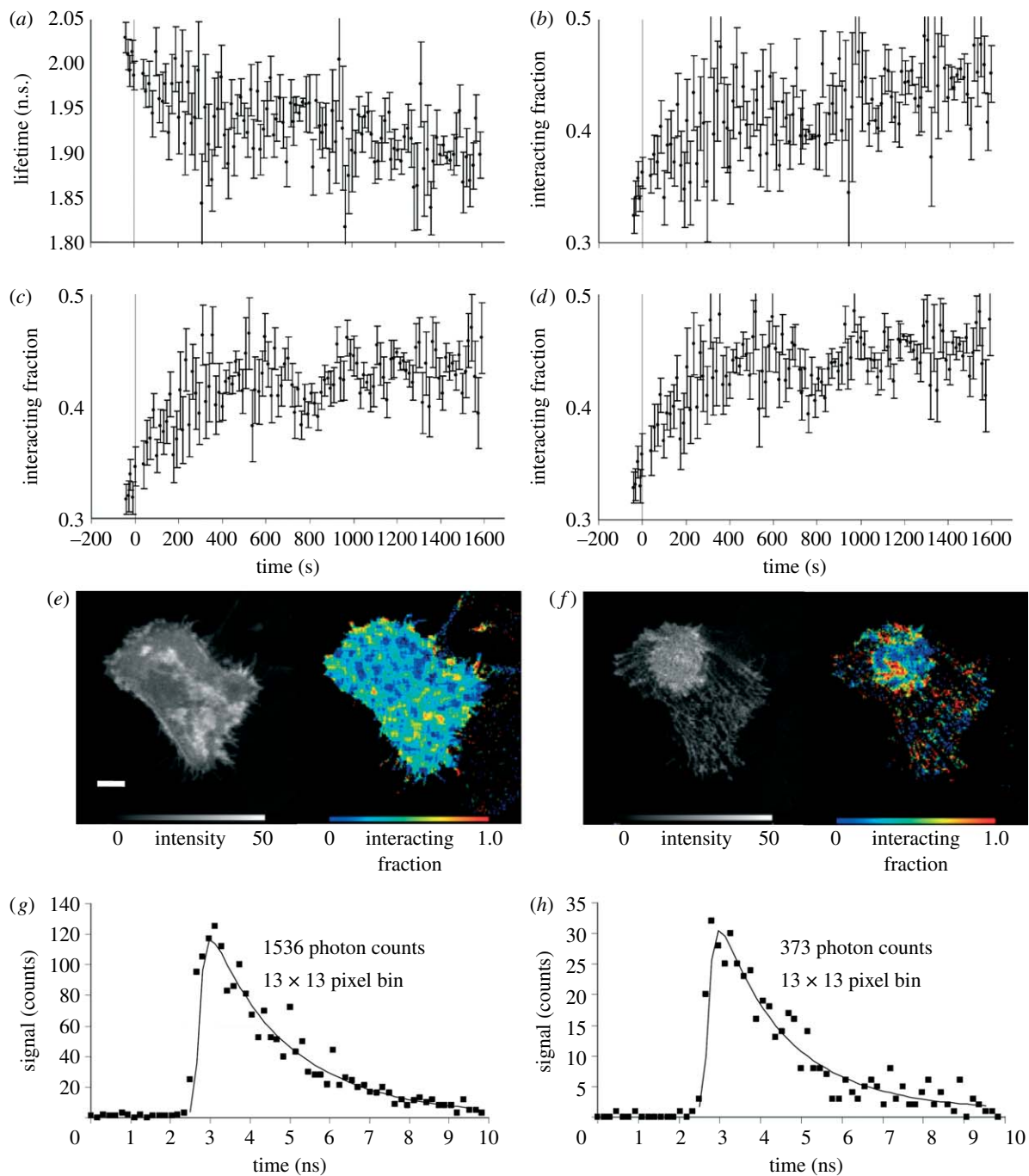
Figure 5. Monitoring Cdc42 activity before and after the addition of EGF (at time zero) using the FRET probe Raichu-Cdc42 in a low-photon-count time-lapse experiment with a short image interval. GFP-only control data were used to derive a non-interacting lifetime of 2.41 ns (see the electronic supplementary material) and this was used to perform bi-exponential fitting. (a) Mono-exponential image-by-image lifetime-invariant fitting reveals a time course in the lifetime suggesting FRET is occurring after time zero. (b) Using lifetime invariant fitting of the whole image sequence (see the electronic supplementary material; experimental and control data), lifetimes in image-by-image invariant fits can be fixed parameters ($\tau_1 = 2.41$ ns, $\tau_2 = 1.36$ ns) revealing a time course in interacting fraction. (c) Spatial information can be retained by pixel binning but only if similarly fixed lifetimes are used. (d) Multi-image global analysis performs equivalent processing on these data in one step and in approximately one-fifth of the processing time revealing a very similar time course and an interacting lifetime of 1.39 ns. Error bars are the standard deviation of the five points around the point of interest. (e, f) Representative before (-15 s) and after (1000 s) images. The scale bar is 20 µm. Interacting fraction maps were derived using multi-image global bi-exponential fits. (g, h) Example transients before and after from 13×13 pixel bins (*dots*), as used in the analysis, and fits (*lines*) with the globally derived lifetime values.

made from a single image makes the global fitting technique amenable to high-throughput and high-content screening applications. Mono-exponential fitting, with appropriate prior knowledge or assumptions, is an alternative which should be used in preference to pixel-by-pixel bi-exponential fitting, approximately when $\eta_{AP} < 0.2$ or $\eta_{AP} > 0.7$ (the actual values depend on the true η_{FRET}). However, when dealing with low photon count, time-lapse data, the assumptions would have to be derived from pixel-binned information, and there are no obvious selection criteria that can be applied in all cases.

In some circumstances, where prior knowledge of component lifetimes is available, more conventional fitting approaches (e.g. lifetime invariant fits) are comparably accurate. However, global analysis approaches, as described, are significantly more robust to varying experimental conditions and less prone to potentially improper manipulation of data by the user. Here, we show that global approaches are valid, as confirmed by comparison with conventional approaches with simulated and experimental data are robust at the extreme of interacting fraction and can be made significantly faster.

In experiments where interfering acceptor fluorescence is present, advantage may come from fitting a tri- or stretched-exponential model such that additional terms can account for the acceptor fluorescence. Any conventional complex exponential fitting would require higher counts in order to be meaningful but this requirement is relaxed and such fitting is easily dealt with using our global analysis technique. The fact that interacting fractions can be derived from transients of only several hundred counts compared with several tens of thousands is indicative of the power of the technique. Additional information on our implementation can be found in table 2 and figures in the electronic supplementary material.

FLIM has the potential to become a potent technique for high-content and high-throughput screening and if this potential is to be realized, it would be beneficial for at least one of two aspects to be improved. First, the speed of acquisition should be increased, without increasing the light exposure of the sample. However, the counting rate of TCSPC hardware is fundamentally limited to a small fraction of the excitation rate and radically different hardware arrangements must be used. Second, processing methods must be improved such that lower photon counts can be tolerated. The algorithms presented in this paper have been targeted to contribute to the second of these requirements.

The FLIM processing of the future may provide fast answers to specific questions for a particular assay, such as indicating if FRET activity has exceeded a given threshold or not. In these cases, fitting a fast mono-exponential model may be preferable, provided sufficient prior knowledge is available and the biological system has been appropriately characterized. Such approaches, coupled with fuzzy reasoning or Bayesian decision making (Ruanaidh & Fitzgerald 1996), may provide fast yes/no answers for screening purposes. When characterizing the biological system, more complex models coupled with global analysis or more exploratory tools, such as phasor plots, may provide slower but more detailed analysis. It is, of course, essential, not to lose sight of the application, but rather to use the appropriate analysis method from the array of approaches available for both time and frequency domains.

REFERENCES

Ameer-Beg, S. M., Barber, P. R., Hodgkiss, R. J., Locke, R. J., Newman, R. G., Tozer, G. M., Vojnovic, B. & Wilson, J. 2002 Application of multiphoton steady state and lifetime imaging to mapping of tumour vascular architecture *in vivo. Proc. SPIE* **4620**, 85–95.

Ameer-Beg, S. M., Edme, N., Peter, M., Barber, P. R., Ng, T. & Vojnovic, B. 2003 Imaging protein–protein interactions by multiphoton FLIM. *Proc. SPIE* **5139**, 180–189. (doi:10.1117/12.500544)

Ameer-Beg, S. M., Peter, M., Keppler, M. D., Prag, S., Barber, P. R., Ng, T. C. & Vojnovic, B. 2005 Dynamic imaging of protein–protein interactions by MP-FLIM. *Proc. SPIE* **5700**, 152–161. (doi:10.1117/12.589202)

Bajzer, Z., Therneau, T. M., Sharp, J. C. & Prendergast, F. G. 1991 Maximum likelihood method for the analysis of time-resolved fluorescence decay curves. *Eur. Biophys. J.* **20**, 247–262. (doi:10.1007/BF00450560)

Barber, P. R., Ameer-Beg, S. M., Gilbey, J., Edens, R. J., Ezike, I. & Vojnovic, B. 2005 Global and pixel kinetic data analysis for FRET detection by multi-photon time-domain FLIM. *Proc. SPIE* **5700**, 171–181. (doi:10.1117/12.590510)

Bastiaens, P. I. H. & Squire, A. 1999 Fluorescence lifetime imaging microscopy: spatial resolution of biochemical processes in the cell. *Trends Cell Biol.* **9**, 48–52. (doi:10.1016/S0962-8924(98)01410-X)

Becker, W. 2005 *Advanced time-correlated single photon counting techniques Chemical physics.* New York, NY: Springer.

Becker, W. *et al.* 2006 Fluorescence lifetime images and correlation spectra obtained by multidimensional time-correlated single photon counting. *Microsc. Res. Technol.* **69**, 186–195. (doi:10.1002/jemt.20251)

Beechem, J. M. & Haas, E. 1989 Simultaneous determination of intramolecular distance distributions and conformational dynamics by global analysis of energy transfer measurements. *Biophys. J.* **55**, 1225–1236.

Benny Lee, K. C., Siegel, J., Webb, S. E. D., Leveque-Fort, S., Cole, M. J., Jones, R., Lever, M. J. & French, P. M. W. 2001 Application of the stretched exponential function to fluorescence lifetime imaging. *Biophys. J.* **81**, 1265–1274.

Chen, Y. & Periasamy, A. 2004 Characterization of two-photon excitation fluorescence lifetime imaging microscopy for protein localization. *Microsc. Res. Technol.* **63**, 72–80. (doi:10.1002/jemt.10430)

Clayton, A. H. A., Hanley, Q. S. & Verveer, P. J. 2004 Graphical representation and multicomponent analysis of single-frequency fluorescence lifetime imaging microscopy data. *J. Microsc.* **213**, 1–5. (doi:10.1111/j.1365-2818.2004.01265.x)

Digman, M. A., Caiolfa, V. R., Zamai, M. & Gratton, E. 2008 The phasor approach to fluorescence lifetime imaging analysis. *Biophys. J.* **94**, L14–L16. (doi:10.1529/biophysj.107.120154)

Eaton, D. F. 1990 Recommended methods for fluorescence decay analysis. *Pure Appl. Chem.* **62**, 1631–1648. (doi:10.1351/pac199062081631)

Esposito, A., Gerritsen, H. C. & Wouters, F. S. 2005 Fluorescence lifetime heterogeneity resolution in the frequency domain by lifetime moments analysis. *Biophys. J.* **89**, 4286–4299. (doi:10.1529/biophysj.104.053397)

Festy, F., Ameer-Beg, S. M., Ng, T. & Suhling, K. 2007 Imaging proteins *in vivo* using fluorescence lifetime microscopy. *Mol. BioSyst.* **3**, 381–391. (doi:10.1039/b617204k)

Gadella, T. W. J., Jovin, T. M. & Clegg, R. M. 1993 Fluorescence lifetime imaging microscopy (FLIM): spatial resolution of microstructures on the nanosecond time scale. *Biophys. Chem.* **48**, 221–239. (doi:10.1016/0301-4622(93)85012-7)

Gerritsen, H. C., Asselbergs, M. A. H., Agronskaia, A. V. & Van Sark, W. G. J. H. M. 2002 Fluorescence lifetime imaging in scanning microscopes: acquisition speed, photon economy and lifetime resolution. *J. Microsc.* **206**, 218–224. (doi:10.1046/j.1365-2818.2002.01031.x)

Gratton, E., Breusegem, S., Sutin, J. & Ruan, Q. Q. 2003 Fluorescence lifetime imaging for the two-photon microscope: time-domain and frequency-domain methods. *J. Biomed. Opt.* **8**, 381–390. (doi:10.1117/1.1586704)

Grinvald, A. & Steinberg, I. Z. 1974 On the analysis of fluorescence decay kinetics by the method of least-squares. *Anal. Biochem.* **59**, 583–598. (doi:10.1016/0003-2697(74)90312-1)

Habenicht, A., Hjelm, J., Mukhtar, E., Bergstrom, F. & Johansson, L. B. A. 2002 Two-photon excitation and time-resolved fluorescence: I. The proper response function for analysing single-photon counting experiments. *Chem. Phys. Lett.* **354**, 367–375. (doi:10.1016/S0009-2614(02)00141-0)

Hall, A. 1998 Rho GTPases and the actin cytoskeleton. *Science* **279**, 509–514. (doi:10.1126/science.279.5350.509)

Hille, C., Berg, M., Bressel, L., Munzke, D., Primus, P., Löhmannsröben, H.-G. & Dosche, C. 2008 Time-domain fluorescence lifetime imaging for intracellular pH sensing in living tissues. *Anal. Bioanal. Chem.* **391**, 1871–1879. (doi:10.1007/s00216-008-2147-0)

Istratov, A. A. & Vyvenko, O. F. 1999 Exponential analysis in physical phenomena. *Rev. Sci. Instrum.* **70**, 1233–1257. (doi:10.1063/1.1149581)

Itoh, R. E., Kurokawa, K., Ohba, Y., Yoshizaki, H., Mochizuki, N. & Matsuda, M. 2002 Activation of Rac and Cdc42 video imaged by fluorescent resonance energy transfer-based single-molecule probes in the membrane of living cells. *Mol. Cell. Biol.* **22**, 6582–6591. (doi:10.1128/MCB.22.18.6582-6591.2002)

Jares-Erijman, E. A. & Jovin, T. M. 2006 Imaging molecular interactions in living cells by FRET microscopy. *Curr. Opin. Chem. Biol.* **10**, 409–416. (doi:10.1016/j.cbpa.2006.08.021)

Jo, J. A., Fang, Q. Y. & Marcu, L. 2005 Ultrafast method for the analysis of fluorescence lifetime imaging microscopy data based on the Laguerre expansion technique. *IEEE J. Sel. Top. Quant. Electron.* **11**, 835–845. (doi:10.1109/JSTQE.2005.857685)

Kollner, M. & Wolfrum, J. 1992 How many photons are necessary for fluorescence-lifetime measurements? *Chem. Phys. Lett.* **200**, 199–204. (doi:10.1016/0009-2614(92)87068-Z)

Kozma, R., Ahmed, S., Best, A. & Lim, L. 1995 The Ras-related protein Cdc42Hs and bradykinin promote formation of peripheral actin microspikes and filopodia in Swiss 3T3 fibroblasts. *Mol. Cell. Biol.* **15**, 1942–1952.

Kurokawa, K., Itoh, R. E., Yoshizaki, H., Ohba, Y., Nakamura, T. & Matsuda, M. 2004 Coactivation of Rac1 and Cdc42 at lamellipodia and membrane ruffles induced by epidermal growth factor. *Mol. Biol. Cell* **15**, 1003–1010. (doi:10.1091/mbc.E03-08-0609)

Lakowicz, J. R. 1999 *Principles of fluorescence spectroscopy.* New York, NY: Plenum Publishers.

Levenberg, K. 1944 A method for the solution of certain non-linear problems in least squares. *Appl. Math.* **2**, 164–168.

Levitt, J. A., Sergent, N., Chauveau, A., Kuimova, M. K., Barber, P. R., Davis, D. M. & Suhling, K. 2008 Multidimensional multiphoton fluorescence lifetime imaging of cells. *Proc. SPIE* **6860**, 68601L. (doi:10.1117/12.763468)

Liu, P., Ahmed, S. & Wohland, T. 2008 The F-techniques: advances in receptor protein studies. *Trends Endocrinol. Metab.* **19**, 181–190. (doi:10.1016/j.tem.2008.02.004)

McConnell, G., Girkin, J. M., Ameer-Beg, S. M., Barber, P. R., Vojnovic, B., Ng, T., Banerjee, A., Watson, T. F. & Cook, R. J. 2007 Time-correlated single-photon counting fluorescence lifetime confocal imaging of decayed and sound dental structures with a white-light supercontinuum source. *J. Microsc.* **225**, 126–136. (doi:10.1111/j.1365-2818.2007.01724.x)

Mizeret, J., Stepinac, T., Hansroul, M., Studzinski, A., Bergh, H. V. D. & Wagnieres, G. 1999 Instrumentation for real-time fluorescence lifetime imaging in endoscopy. *Rev. Sci. Instrum.* **70**, 4689–4701. (doi:10.1063/1.1150132)

Nakagawa, A., Kobayashi, N., Muramatsu, T., Yamashina, Y., Shirai, T., Hashimoto, M. W., Ikenaga, M. & Mori, T. 1998 Three-dimensional visualization of ultraviolet-induced DNA damage and its repair in human cell nuclei. *J. Invest. Dermatol.* **110**, 143–148. (doi:10.1046/j.1523-1747.1998.00100.x)

Ng, T. *et al.* 1999 Imaging protein kinase C alpha activation in cells. *Science* **283**, 2805–2809. (doi:10.1126/science.283.5410.2085)

Parsons, M. *et al.* 2005 Spatially distinct binding of Cdc42 to PAK1 and N-WASP in breast carcinoma cells. *Mol. Cell Biol.* **25**, 1680–1695. (doi:10.1128/MCB.25.5.1680-1695.2005)

Pelet, S., Previte, M. J. R., Laiho, L. H. & So, P. T. C. 2004 A fast global fitting algorithm for fluorescence lifetime imaging microscopy based on image segmentation. *Biophys. J.* **87**, 2807–2817. (doi:10.1529/biophysj.104.045492)

Periasamy, N. 1988 Analysis of fluorescence decay by the nonlinear least squares method. *Biophys. J.* **54**, 961–967.

Peter, M. & Ameer-Beg, S. M. 2004 Imaging molecular interactions by multiphoton FLIM. *Biol. Cell* **96**, 231–236. (doi:10.1016/j.biolcel.2003.12.006)

Philip, J. & Carlsson, K. 2003 Theoretical investigation of the signal-to-noise ratio in fluorescence lifetime imaging. *J. Opt. Soc. Am. A* **20**, 368–379. (doi:10.1364/JOSAA.20.000368)

Prag, S. *et al.* 2007 Activated ezrin promotes cell migration through recruitment of the GEF Dbl to lipid rafts and preferential downstream activation of Cdc42. *Mol. Biol. Cell* **18**, 2935–2948. (doi:10.1091/mbc.E06-11-1031)

Ridley, A. J. 2006 Rho GTPases and actin dynamics in membrane protrusions and vesicle trafficking. *Trends Cell Biol.* **16**, 522–529. (doi:10.1016/j.tcb.2006.08.006)

Rolinski, O. J., Birch, D. J. S., McCartney, L. J. & Pickup, J. C. 2000 A method of determining donor–acceptor distribution functions in Forster resonance energy transfer. *Chem. Phys. Lett.* **324**, 95–100. (doi:10.1016/S0009-2614(00)00577-7)

Ruanaidh, J. & Fitzgerald, W. J. 1996 *Numerical Bayesian methods applied to signal processing Statistics and computing.* New York, NY: Springer.

Shaner, N. C., Steinbach, P. A. & Tsien, R. Y. 2005 A guide to choosing fluorescent proteins. *Nat. Methods* **2**, 905. (doi:10.1038/nmeth819)

Sharman, K. K., Periasamy, A., Ashworth, H., Demas, J. N. & Snow, N. H. 1999 Error analysis of the rapid lifetime determination method for double-exponential decays and new windowing schemes. *Anal. Chem.* **71**, 947–952. (doi:10.1021/ac981050d)

Tadrous, P. J. 2000 Methods for imaging the structure and function of living tissues and cells: 2. Fluorescence lifetime imaging. *J. Pathol.* **191**, 229–234. (doi:10.1002/1096-9896(200007)191:3<229::AID-PATH623>3.0.CO;2-B)

Verveer, P. J. & Bastiaens, P. I. H. 2003 Evaluation of global analysis algorithms for single frequency fluorescence lifetime imaging microscopy data. *J. Microsc.* **209**, 1–7. (doi:10.1046/j.1365-2818.2003.01093.x)

Verveer, P. J., Squire, A. & Bastiaens, P. I. H. 2000 Global analysis of fluorescence lifetime imaging microscopy data. *Biophys. J.* **78**, 2127–2137.

Voss, T. C., Demarco, I. A. & Day, R. N. 2005 Quantitative imaging of protein interactions in the cell nucleus. *Biotechniques* **38**, 413–424. (doi:10.2144/05383RV01)

Wallrabe, H. & Periasamy, A. 2005 Imaging protein molecules using FRET and FLIM microscopy. *Curr. Opin. Biotechnol.* **16**, 19–27. (doi:10.1016/j.copbio.2004.12.002)

Woods, R. J., Scypinski, S. & Love, L. J. C. 1984 Transient digitizer for the determination of microsecond luminescence lifetimes. *Anal. Chem.* **56**, 1395–1400. (doi:10.1021/ac00272a043)

Wouters, F. S. & Esposito, A. 2008 Quantitative analysis of fluorescence lifetime imaging made easy. *HFSP J.* **2**, 7–11. (doi:10.2976/1.2833600)

Wouters, F. S., Verveer, P. J. & Bastiaens, P. I. H. 2001 Imaging biochemistry inside cells. *Trends Cell Biol.* **11**, 203–211. (doi:10.1016/S0962-8924(01)01982-1)